Structural Engineering and Mechanics, *Vol. 60, No. 4 (2016) 567-594*
DOI: http://dx.doi.org/10.12989/sem.2016.60.4.567

Structural performance of ribbed ferrocement plates reinforced with composite materials

Yousry B.I. Shaheen[1a], Ashraf M. Mahmoud[*2] and Hala M. Refat[3b]

[1]*Civil Engineering Department, Faculty of Engineering, Menoufia University, Menoufia, Egypt*
[2]*Civil Engineering Department, Faculty of Engineering, Modern University for Technology and Information (MTI), Al-Mokattam, Cairo, Egypt*
[3]*Civil Engineering Department, Faculty of Engineering, Benha University, Benha, Egypt*

(Received January 8, 2016, Revised July 13, 2016, Accepted July 28, 2016)

Abstract. The main objective of the current research is estimating the flexural behavior of ferrocement Ribbed Plates reinforced with composite material. Experimental investigation was carried out on fifteen plates; their dimensions were kept constant at 1200 mm in length, 600 mm width and 100 mm thick but with different volume fraction of steel reinforcement and number of ribs. Test specimens were tested until failure under three line loadings with simply supported conditions over a span of 1100 mm. Cracking patterns, tensile and compressive strains, deformation characteristics, ductility ratio, and energy absorption properties were observed and measured at all stages of loadings. Experimental results were compared to analytical models using ANSYS 10 program. Parametric study is presented to look at the variables that can mainly affect the mechanical behaviors of the model such as the change of plate length. The results showed that the ultimate strength, ductility ratio and energy absorption properties of the proposed ribbed plates are affected by the volume fraction and the type of reinforcement, and also proved the effectiveness of expanded metal mesh and woven steel mesh in reinforcing the ribbed ferrocement plates. In addition, the developed ribbed ferrocement plates have high strength, ductility ratio and energy absorption properties and are lighter in weight compared to the conventional RC ribbed plates, which could be useful for developed and developing countries alike. The Finite Element (FE) simulations gave good results comparing with the experimental results.

Keywords: ferrocement; ribbed plates; composite material; experimental; FE modeling; Ansys 10; parametric study

1. Introduction

Ferrocement concrete, large amounts of small-diameter wire meshes are used instead of reinforcing bars and in which Portland cement mortar is used instead of concrete in the reinforced concrete. Ferrocement is reinforced with a wide variety of metallic reinforcing mesh materials; woven wire mesh, welded wire mesh and expanded metal mesh. Ferrocement has been used for at

∗Corresponding author, Lecturer, E-mail: ashraf_amin78@yahoo.com
[a]Professor, E-mail: Ybishaheen@yahoo.com
[b]Lecturer, E-mail: hala.abusafa@bhit.bu.edu.eg

http://www.techno-press.org/?journal=sem&subpage=8 ISSN: 1225-4568 (Print), 1598-6217 (Online)

least 150 years in boats industry.

Ferrocement material has been defined by ACI 249R-93 (1993) as "A type of reinforced concrete commonly constructed of hydraulic cement mortar reinforced with closely spaced layers of relatively small wire diameter mesh. The mesh may be made of metallic or other suitable materials. The fineness of the mortar matrix and its composition should be compatible with the opening and tightness of the reinforcing system it is meant to encapsulate. The matrix may contain discontinuous fibers".

Due to the many researches that were conducted on ferrocement technology, recently the applications of ferrocement have become versatile such as different roofing systems, retaining walls, sculptures, bus shelters, bridge decks, repair works, water structures like tanks, strengthening and precast ferrocement elements (Aboul-Anen, El-Shafey *et al*. 2009, Ali 1995, Al-Kubaisy and Jumaat 2000, Robles-Austriaco, Pama *et al.* 1981, Elavenil and Chandrasekar 2007, Fahmy, Shaheen *et al.* 1997).

Many investigators have reported the advantages of ferrocement in comparing with the conventional reinforced concrete. In addition, numerous test data are available to define its performance criteria for construction and repair of structural elements (Fahmy and Shaheen 1994, Fahmy, Shaheen *et al.* 1999, Fahmy, Ezzat *et al.* 2004, 2005). From these investigations, it can be concluded that ferrocement has features included ease of prefabrication and low cost in maintenance and repair. Compared with the conventional reinforced concrete, ferrocement is reinforced in two directions (with wire meshes) so that it has homogenous-isotopic properties in the two directions. In addition, ferrocement generally has a high tensile strength and a high modulus of rupture because that it usually benefits with its high reinforcement ratio. Additionally, because the specific surface of reinforcement of ferrocement is one to two orders of magnitude higher than that of reinforced concrete, larger bond forces develop with the matrix resulting in average crack spacing and width more than one order of magnitude smaller than in conventional reinforced concrete (Jumaat and Alam 2006, Kaish, Alam *et al.* 2012, Mourad and shang 2012, Xiong, Wu *et al.* 2011, El-Sakhawy 2000, El-Halfawy 2003, Shaheen, Safan *et al.* 2013, Al-Rifaei and Hassan 1994). Sakthivel and Jagannathan (2012) investigated a new non-corrosive mesh material in ferrocement; PVC-coated steel welded mesh. Then Sakthivel and Jagannathan (2012) studied a low-velocity impact study on square fibrous ferrocement slab (250 mm length and 25 mm thickness) reinforced with PVC-coated welded mesh. Their results indicated that the impact energy increases with increasing in the number of mesh layers. Hafiz (2012), Shaheen, Soliman *et al.* (2013) studied the structural behavior of fourteen ferrocement channel beams under four point loadings until failure. The beams reinforced with various types of meshes; welded, expanded and fiberglass meshes. Their results indicated that the beam reinforced with welded wire mesh achieved higher first crack load, serviceability load, ultimate load and energy absorption than beams reinforce with expanded and fiberglass mesh. Abdul-Fataha (2014), Shaheen, Eltaly *et al.* (2014) designed an experimental program and employed numerical models to examine the structural behavior of twelve ferrocement beams under three point loadings up to failure. The twelve beams were different in the type of reinforcements; steel bars, traditional wire meshes (welded and expanded wire meshes) and composite materials (fiberglass wire meshes and polypropylene wire meshes). The results of the experimental tests and numerical models concluded that the beam with fiberglass meshes gives the lowest first crack load and ultimate load. In addition, their results indicated that the ferrocement beam reinforced with four layers of welded wire meshes has better structural behavior than those beams reinforced with other types of wire meshes. Shannag and Mourad (2012) developed high strength mortar matrices contain

various combinations of silica fume and fly ash, and provide a good balance between workability and strength. Mourad and Shang (2012) used ferrocement jacket in repairing reinforced concrete column. Their test results indicated that using the ferrecement jacket increases the axial load capacity and the axial stiffness of repaired reinforced concrete column compared to the control columns.

Many investigators (Fahmy and Shaheen 1994, Fahmy, Shaheen *et al.* 1999, Fahmy, Shaheen *et al.* 2004, Fahmy, Shaheen *et al.* 2005) have reported the physical and mechanical properties of ferrocement material and numerous test data are available to define its performance for construction and repair of structural elements.

The results of an experimental investigation of the feasability of using ferrocement as a low permeability cover layer to reinforced concrete members located in a high risk of reinforcement corrosion environments were presented (Mays and Barnes 1995). The desirable mix proportions of the mortar for ferrocement are sand/cement ratio by weight, (1.5 to 2.5), and water/cement ratio by weight, (0.30 to 0.5). These mix proportions will produce a satisfactory matrix that occupies about 95% of the total volume of the ferrocement layer.

There is a wide variety of metallic reinforcing mesh materials, yet steel mesh is the most common used type with its various shapes such as woven or interlocking mesh, welded wire mesh, expanded metal lath, and punched or perforated sheets. Meshes made of alkali-resistant glass fibers such as jute burlap and bamboo has also been tried. Sometimes, regular reinforcing bars in a skeletal form are added to the thin wire meshes in order to achieve a stiff reinforcing cage.

There are major differences between conventional reinforced concrete and ferrocement elements are normally thin with a thickness that rarely exceeds (25 mm). On the other hand, conventional concrete members are relatively thick sections that often exceed (100 mm). The ferrocement matrix mainly consists of Portland cement mortar instead of regular concrete that contains coarse aggregates. The reinforcement provided in ferrocement consists of large amount of smaller-diameter wires or meshes instead of discretely placed reinforcing bars used in reinforced concrete. Moreover, ferrocement normally contains a greater percentage of reinforcement distributed throughout the cross-section. Several factors have contributed to the wide spread use of ferrocement, its mechanical properties, the possibility of using elements without using formwork, high impact resistance and toughness, the economic advantages due to produced element thickness, durability, crack resistance and simplified repair operations.

The behavior of ferrocement channel beams under four point loadings until failure is investigated (Shaheen, Safan *et al.* 2013). The beams reinforced with various types of meshes; welded, expanded and fiberglass meshes. Their results indicated that the beam reinforced with welded wire mesh achieved higher first crack load, serviceability load, ultimate load and energy absorption than beams reinforced with expanded and fiberglass mesh.

The effect of the strength of ferrocement jackets for initially damaged exterior RC beam-column joints is presented (Singh, Bansal *et al.* 2015). In this study, the experimental observation showed improvement in ultimate load, yield load carrying capacity with increase in stiffness of the ferrocement-jacketed joints in comparison to control joint.

The improvement of the practical use of the ferrocement I-beams by attempting to develop its ductile behavior is investigated. The evaluation of the actual flexural capacity of the ferrocement I-beam with additional layers of wire mesh in the flange section as compared to the theoretical analysis computation is illustrated (Acma, Dumpasan *et al.* 2015). The design and construction of the ferrocement channels were presented with various materials (e.g., meshes and mortar). In addition, an optimal combination of meshes was obtained and finite element FE models of the channels were implemented using ABAQUS Unified FEA (Eskandari and Madadi 2015).

The objective of the current paper is to examine the flexural behavior of Ribbed Ferrocement Plates reinforced with composite material; expanded metal mesh and woven steel mesh, and comparing their behavior with ferrocement plates reinforced with traditional steel reinforcement.

Fifteen plates with different volume fraction of steel reinforcement and number of ribs were tested up to failure. In addition, the current research aims to simulate the tested plates by finite element ANSYS 10 program to investigate their flexural behavior up to failure.

2. Experimental program

The experimental program included constructing and testing of 15 plates 1200 mm long, 600 mm wide and 100 mm total thickness. Seven designations series were developed. Series 1 consisted of casting and testing two conventional concrete plates. Series 2 comprised casting and testing of plates No. 3 and 4 which were reinforced with one layer and two layers of X8 expanded steel mesh incorporating two and four skeletal steel bars in the longitudinal direction respectively. Series 3 consisted of casting and testing of plates No. 5 and 6 which were reinforced with one layer and two layers of woven square steel mesh of size of opening 25 mm and wire diameter 2.7 mm, two and four skeletal steel bars were used in the longitudinal direction respectively. Series 4 consisted of casting and testing of plates No. 7 and 8. Plate 7 included two ferrocement ribs of 50 mm width and the 80 mm thick light brick; the ferrocement layer was tied with the brick by using shear connectors. Plate No. 8 was designed incorporating, two skin layers of 20 mm thick at the top and bottom of the plates. In series designation 5 two plates were cast and tested, plates 9 and 10 where the same design mentioned in series 4 was followed but with using three ferrocement ribs. Series designation 6 comprises casting and testing of ribbed ferrocement plates with four ribs. In series designation seven, three plates 13, 14 and 15 were cast and tested. Plate No 13 was designed with two ribs, plate No. 14 was designed with three ribs and finally plate No 15 was manufactured with four ferrocement ribs. The main variables studied were the number of reinforcing mesh layers, type of mesh used, volume fraction of reinforcing steel, combination of mesh and skeletal steel bars, employing light brick as core material and to study the effect of increasing the number of webs in the structural behavior of ferrocement plates. All test specimens were tested under three line loadings with simply supported over a span of 110 cm until failure. All the deformation characteristics, cracking patterns and strengths were measured at all stages of loadings. Fig. 1 shows cross sections of the tested plates. Their details are given in Table 1.

2.1 Material properties

2.1.1 Cement

Ordinary Portland cement was used throughout this work (O.P.C) with a specific surface area (Blaine fineness) of 3050 cm^2/gm. Typical compounds of the cement was as follows: C3S=65.1 percent, C2S=7.6 percent, C3A=10.8 percent and C4AF=7.3 percent. The alkali content (as Na2O equivalent) was 0.29 mass percent.

2.1.2 Silica fume

Silica fume (S.F.) was employed in the present work to enhance the strength of ferrocement mortar and/or concrete core. It was used as partial replacement by weight of cement in the mortar mixtures. The S.F. had an average particle size of 0.1 micrometer and a silicon dioxide content of 93%.

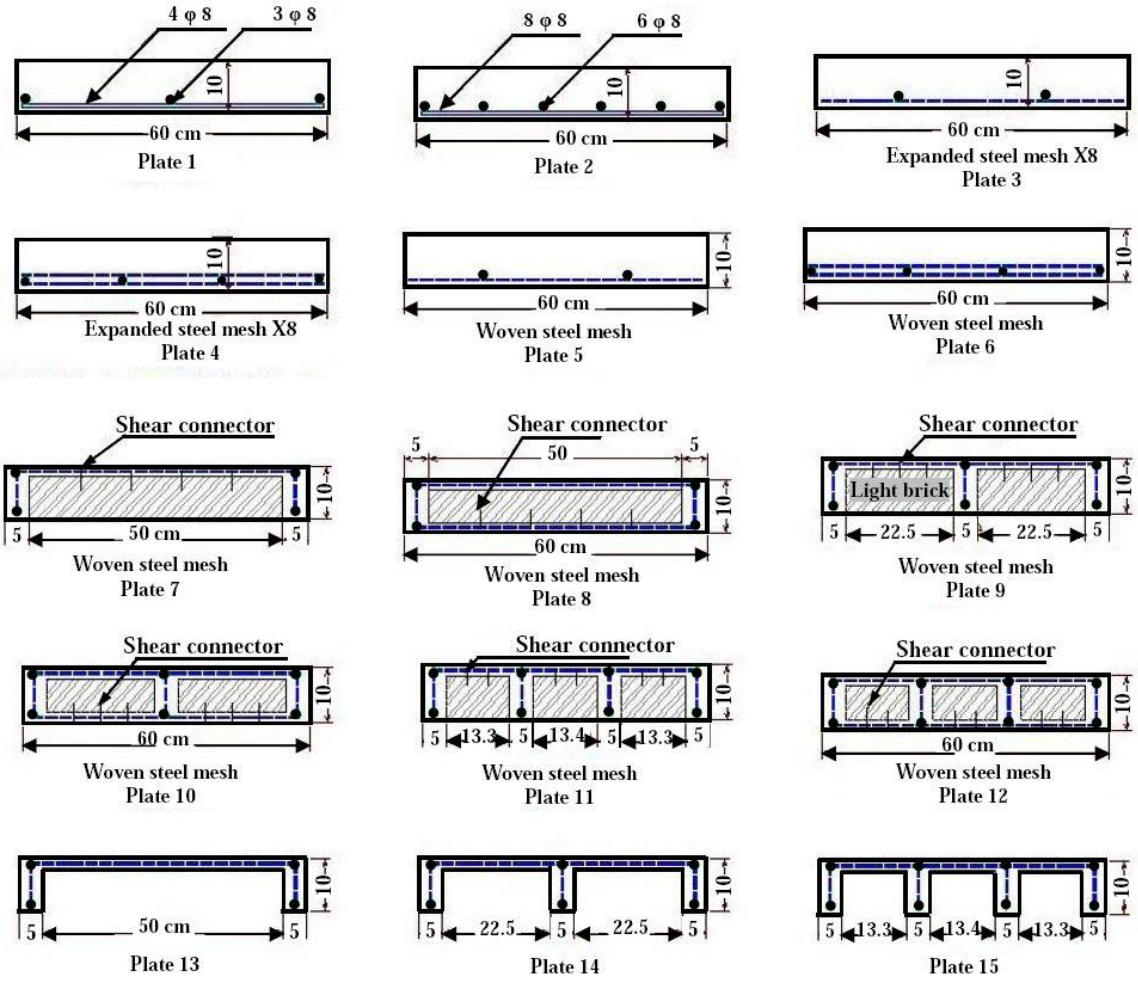

Fig. 1 Cross sections of the tested Plates

2.1.3 Fine aggregates

Natural siliceous sand with a fineness modulus of 2.91, a saturated surface dry specific gravity of 2.51 and absorption of 0.50 percent was used in the present experimental work.

2.1.4 Plasticizer (Water-reducer)

A water reducing admixture was used to produce mortar and concrete of high workability with lower water to cement ratios. According to the product data sheet provided by the manufacturer, it complies with ASTM C494 type F and BS 5075 part 3. Its base material is Naphthalene Formaldehyde Sulphonate and has a density of 1.200±0.005 Kg/l at 20℃. The manufacturer is recommended dosage is between 0.6% to 3% by weight of cement, depending on the desired workability and strength.

2.1.5 Expanded steel mesh

Expanded wire steel mesh X8 diamond size 9.5×31 mm and weight 2.54 Kg/m^2, Fig. 2 was

Table 1 Details of the tested plates

Series Designations	Plate No.	No. of Layers of Refinement At each face	Longitudinal Reinforcement			Core material
			Type of reinforcement	Volume Fraction (V_{rL})		
				In the Ferrocement Layer	In each web	
A	PL1	------	Steel bars	0.0042	------	------
	PL2		D = 8 mm	0.0084	------	------
B	PL3	1	Expand. X8*	0.0062	------	------
	PL4	2		0.0124		
C	PL5	1	W.S.M**	0.0064	------	------
	PL6	2		0.0128		
D	PL7	1	W.S.M	0.0220	0.000097	LB***
	PL8	2		0.0258	0.000097	LB
E	PL9	1	W.S.M	0.0270	0.000097	LB
	PL10	2		0.0300	0.000097	LB
F	PL11	1	W.S.M	0.0270	0.000097	LB
	PL12	2		0.0300	0.000097	LB
G	PL13	1	W.S.M	0.0226	0.000097	------
	PL14			0.0270	0.000097	
	PL15			0.0303	0.000097	

* Expanded steel mesh X8
** Woven steel mesh
*** Light weight brick.

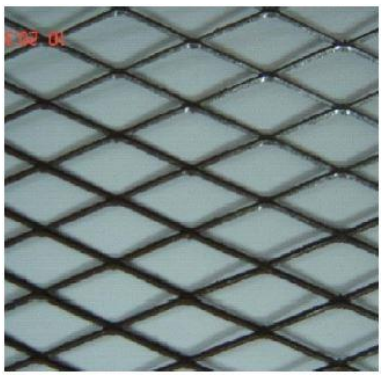

Fig. 2 Expanded metal mesh, X8

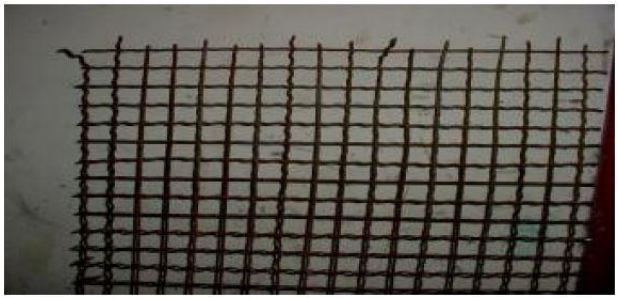

Fig. 3 Woven steel mesh

used to reinforce the ferrocement plates as shown in Table 1. The mesh has a proof stress of 207 MPa, ultimate strength of 250 MPa. and modulus of elasticity 120 Gpa

2.1.6 Woven wire mesh

Woven wire steel mesh of 2.7 mm diameter and opening size of 25x25 mm, Fig. 3, was used to reinforce some of the ferrocement plates as shown in Table 1. The mesh has a proof stress of 243 MPa and ultimate strength of 277 MPa and modulus of elasticity 170 GPa.

2.1.7 Steel reinforcement

Mild steel bars of diameter 8mm were used to reinforce the plates. Tensile tests were performed on three samples of the bars and indicated an average yield stress of 278 MPa and ultimate strength of 457 MPa.

2.2 Mix design

The materials used for the mix design were ordinary Portland cement, sand, silica fume and a super plasticizing agent. The main objectives of mix design was to determine the high amount of cement could be partially replaced by silica fume to increase strength of mortar matrix with no detrimental effects on the quality and properties of the mix in both the fresh and hardened states. The requirement of good workability was essential, to allow the mortar matrix to penetrate through the layers of steel mesh reinforcement. A super plasticizing agent was used to increase flow characteristics and accelerate the early strength development. Mortar mixtures for the ferrocement were made using a water to cement ratio of 0.4, sand to cement ratio of 2:1 and super-plasticizer of 2% by weight of cement, while 10% by weight of cement was replaced by S.F. The density of the mortar mix was approximately 2200 kg/m^3. The average compressive strength after 28 days was 35 MPa.

2.3 Preparation of test specimens

For casting concrete plates a special strong mould was designed. It consisted of 20 mm thick wooden sheet covered with aluminum thin sheet of 3 mm thickness, which made observation of cracks during early ages easier. Four aluminum side angles were screwed to the composite wooden plate with the dimensions required of the specimen. Fine holes were located in the side angles to allow fine steel wires to be threaded through into the holes. Set screws with holes were used to tension these wires by means of lock nuts. The reinforcing cage was supported on these wires. The ferrocement forms were left for 24 hours in the mould before deassembling the mould.

2.4 Test setup

A built up strong testing steel frame was used and provided with hydraulic jack and load cell to measure the applied load. To simulate a simple support, two horizontal circular steel bars of 50 mm diameter were welded in the base of the vertical steel frame. Rubber pads of 20 mm wide and 4 mm thick were fitted at the top of the bars with their center lines coincided with the bars. Fig. 4

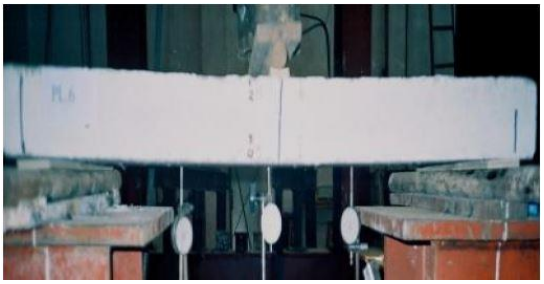

Fig. 4 Test setup

shows the test setup. A set of eight "demec" points was placed on one side of the test plates to allow measuring the strain versus load during the test. A mechanical strain gauge reader of 100 mm gauge was used for recording both compressive and tensile strains with high accuracy. Three dial gauges were used for measuring the deflection at three points. Crack width measurements were made by using a 80X magnification internally illuminated microscope fitted with a micrometer that has the accuracy of one micron. The maximum reading that could be measured was 3 mm. Load, deflection, compressive mortar strains, tensile mortar strains and crack width measurements were taken from first application of load up to failure.

3. Finite element simulation

A general purposed finite element program, ANSYS 10, was used in the current research to simulate the tested ribbed ferrocement plates theoretically. Solid65 elements were used for modeling mortar and the wire meshes. Each element is defined by eight nodes. Each node has three degrees of freedom (translations in the nodal *x*, *y*, and *z* directions). This element has one solid material and up to three rebar materials in the three directions. The solid material is used to model the mortar. The rebar capability is used for modeling wire mesh. The wire mesh is specified by its material, volume ratio and orientation angles. The volume ratio is defined as the rebar volume divided by the total element volume. The orientation is defined by two angles in degrees (θ and φ) from the element coordinate system as shown in Fig. 5. This element has the ability of cracking (in the three orthogonal directions), crushing, plastic deformation, and creep (ANSYS 20 06, Hoque 2006, Singh 2006, Shaheen, Safan *et al.* 2013). An eight-node solid element, Solid 45, was used to model the steel plates under the load. The element is defined with eight nodes having three degrees of freedom at each node in the nodal x, y, and z directions. The geometry and node locations for this element type are shown in Fig. 6. Steel bars and stirrups were modeled by link8 elements. Link8 is a uniaxial tension-compression element with three degrees of freedom at each node: translations in the nodal *x*, *y*, and *z* directions. Plasticity, creep, swelling, stress

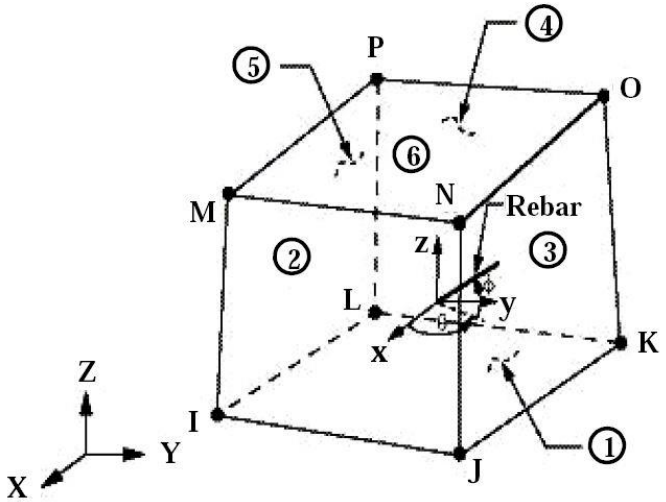

Fig. 5 Solid65-3D solids modeling

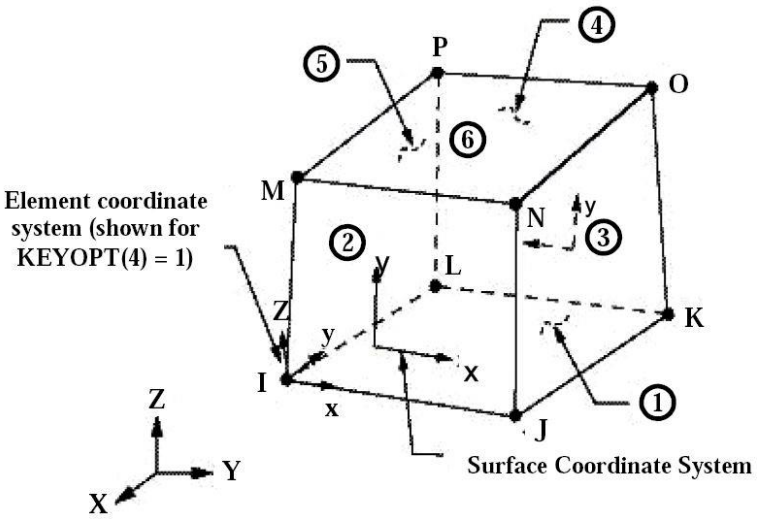

Fig. 6 Solid45-3D solids modeling

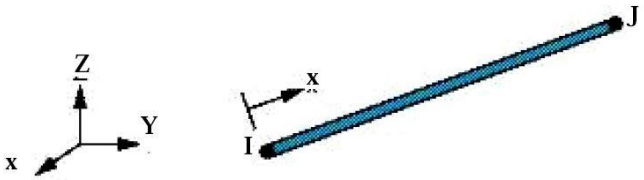

Fig. 7 Link8-3D spar modeling

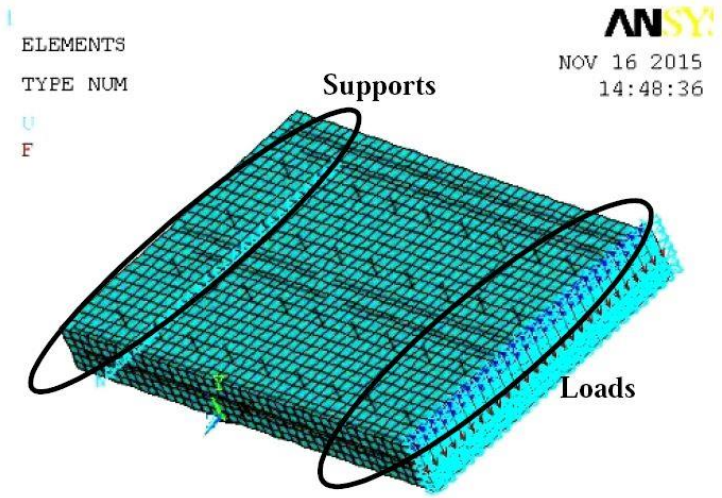

Fig. 8 FE simulation of the half tested plate PL7

stiffening, and large deflection capabilities are included. A schematic of the element was shown in Fig. 7. Each support was presented by 27-hinged supports. The load was concentrated at

27 joints at the mid-span of the analyzed plates as indicated in Fig. 8.

The material of the mortar is defined by the compressive, tensile strength of concrete after 28 days, the modulus of elasticity and the multi-linear isotropic stress-strain curve. The modulus of elasticity of concrete and stress-strain curve were employed the Egyptian Code (2007). The modulus of elasticity of concrete (E_C in MPa) can be calculated from Eq. (1) by considering the compressive strength of concrete after 28 days (F_{CU} in MPa). The multi-linear isotropic stress-strain curve for the concrete can be computed by Eqs. (2) and (3). The stress-strain curve of the used ferrocement mortar in all tested plates is considered as 12.8 GPa as presented in Fig. 9(a), except for the control plates PL1 and PL2, the modulus of elasticity is considered as 11.8 GPa as presented in Fig. 9(b). The steel and the wire meshes were defined by the yield stress and the modulus of elasticity as illustrated in the experimental program section.

$$E_c = 4400\sqrt{F_{cu}} \tag{1}$$

$$stress = \frac{E_c \varepsilon}{1 + \left(\varepsilon / \varepsilon 0\right)^2} \tag{2}$$

$$\varepsilon_o = \frac{2F_{cu}}{E_c} \tag{3}$$

4. Results and discussion

4.1 Experimental results

Table 2 shows the experimental results of all test specimens. It is clear from these results that using woven steel mesh and expanded metal mesh in reinforcing the ferrocement plates in series designations B and C is very effective in increasing their ultimate load than the conventional reinforcements. The ultimate load of plates 3 and 5 is higher than that of plate 1 in series A by approximately 96 and 21% respectively, while the ultimate load of plates 4 and 6 is higher than that of plate 2 in series A by 67 and 47% respectively. In series designation D, plate 8 which was composed of one layer of ferrocement in compression and other layer of ferrocement in tension and in-between a core of light weight brick of thickness 6 cm attained ultimate load of is 30 kN which is about 2.2 times that of plate 7. This could be attributed to the effect of the ferrocement layer in tension zone of the plate. Comparing the experimental ultimate load of plates 7 and 9, it is interesting to note that by increasing the number of ribs from two to three resulted in increasing the ultimate load of plate 9 to be approximately 180% of that of plate 7. Comparing the ultimate load of plate 12, where the number of ribs was increased to four, with that of plate 10 shows that the ultimate load of plate 12 is equal to about 174% of that of plate 10. This shows that increasing the number of ribs and consequently the rib reinforcement has an influence in increasing the ultimate load of the plate. Finally in series designation G the ultimate loads of plates 13, 14 and 15 were equal to 11.2, 14.6, and 16.8 kN respectively. It is worth noting that by increasing the number of ribs of plate 15 to four the ultimate load of that plate is about 1.5 of that of plate 13, where the number of ribs was equal to two.

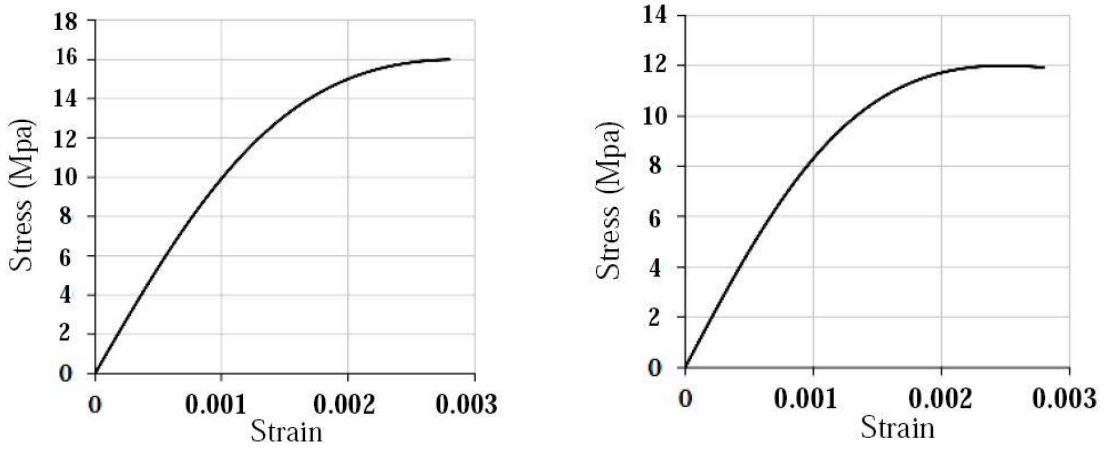

(a) Mortar stress-strain curve of all plates (b) Mortar stress-strain curve of plates PL1 and PL2

Fig. 9 Stress-strain curve of ferrocement mortar

Table 2 Test results for all test specimens

Designation	Plate No.	Volume Fraction	First Crack load (kN)	Serviceability Load* (kN)	Ultimate Load (kN)	First Crack Deflection (mm)	Deflection at Serviceability Load (kN)	Maximum deflection (mm)	Ductility Ratio	Energy Absorption (kN.mm)
A	PL1	0.0042	8.00	7.70	14.5	1.8	1.3	35.4	19.9	563.50
	PL2	0.0084	15.4	17.3	30.0	2.6	2.9	27.3	10.6	689.50
B	PL3	0.0062	20.0	16.4	28.5	2.5	2.0	16.8	6.8	417.40
	PL4	0.0124	20.0	42.8	50.0	3.1	4.7	15.3	4.9	705.60
C	PL5	0.0064	8.00	9.50	17.5	1.4	1.8	17.7	12.6	312.40
	PL6	0.0128	20.0	26.1	44.0	2.7	3.7	48.5	17.8	1883.0
D	PL7	0.0220	12.0	7.70	13.5	6.3	2.7	15.7	2.50	324.50
	PL8	0.0258	24.0	17.8	30.0	6.0	3.5	11.0	1.80	602.90
E	PL8	0.0270	14.0	14.4	24.5	3.7	3.8	14.0	3.80	497.20
	PL10	0.0300	16.0	15.6	26.5	4.3	4.2	20.9	4.80	709.40
F	PL11	0.0270	14.0	16.6	28.0	2.9	3.5	11.4	4.00	467.30
	PL12	0.0300	34.0	27.7	46.0	5.3	3.8	14.4	2.70	947.90
G	PL13	0.0226	6.00	6.50	11.2	4.0	4.4	23.3	5.80	225.20
	PL14	0.0270	8.00	8.80	14.6	4.2	4.6	15.7	3.70	311.50
	PL15	0.0303	18.0	9.70	16.8	4.4	4.3	17.7	4.00	449.60

* Serviceability load according to CP110, $P_{service}=(P_{ult}–1.4\ D.L)\ /\ 1.6$

4.1.1 Deflection and ductility ratio

All tested plates showed typical three-stage load versus mid-span deflection relationship. Under initial loading the load-deflection response was linear up to cracking load. The second stage is

defined by cracking section behavior with the steel reinforcement behaving linear elastic. Transition into third phase of behavior is marked by yielding of the tensile reinforcement and non-linear material behavior. After yielding of tension steel, plate behavior is defined by large increase in deformation with little increase in applied load. As a result, all tested plates showed large deflection at ultimate loading, which is an indication of high ductility. Fig. 10 shows the load deflection curves at mid-span of the tested plates.

Table 2 summarized comparison of deflections at first crack, serviceability loads based on CP110, and ultimate loads. It is worth noting that the value of deflections at the serviceability loads for plates in series C, D, E, and F were less than the limit of 4.4 mm and this is predominant. On other hand, it is interesting to note from Table 2 that the highest ductility ratio was found to be 19.9 for plate 1 in series designation A, reinforced by mild steel bars without any steel mesh reinforcement. Additionally, the plates reinforced with woven steel mesh (series C) achieved higher ductility as compared to those reinforced with expanded steel mesh (series B). Also, it can be concluded that the ductility ratios for plates in series designation B were varied from 6.8 for plate 3 to 4.9 for plate 4, reinforced with expanded metal mesh X8 and mild steel bars as tensile reinforcement, while ductility ratios for plates in series designation C, which were reinforced with woven steel mesh and mild steel bars were found to be 12.6 for plate 5 and 17.8 for plate 6. One can observed that the increasing in the number of ribs from two to three resulted in increasing the ductility ratio for the plates with light brick core. This can be seen from comparing the results of series D (2.5 and 1.8 for plates 7 and 8 respectively) with the corresponding plates of series E (3.8 and 4.8 for plates 9 and 10 respectively). Moreover, for series designation F, plates 11 and 12, which comprise layers of ferrocement, light brick core, and four ferrocement ribs, the ductility ratios were 4.0 and 2.7 respectively. For series designation G, plates 13, 14 and 15, which comprise layers of ferrocement, without light brick core, two, three, and four ferrocement ribs respectively, the ductility ratios, were found to be 5.8, 3.7, and 4.0 respectively.

4.1.2 Energy absorption

The experimental program was carefully undertaken with high accuracy. Three dial gauges were calibrated and located underneath of the test specimens until failure. Energy absorption was calculated as the total area under load deflection curve until failure by using simple designed computer program. The experimental results given in Table 2 show that as the volume fraction of reinforcement in the ferrocement plates increase, energy absorption also increased. It is interesting to note from Table 2 that for plates in series designation A, reinforced by mild steel bars without any mesh reinforcement, the energy absorption was 563.5 and 689.5 kN.mm for plates 1 and 2 respectively. Additionally, for plates in series designation B plate 3 and 4, energy absorptions were 417.4 and 705.6 kN.mm respectively. For plates in series designation C plates 5 and 6, energy absorptions were 312.4 and 1883.0 kN.mm respectively. In general, the results show that increasing the number of ribs resulted in increasing energy absorption. This is observed by comparing the results of plates 7, 9 and 11, where the energy absorptions were 324.5, 497.2 and 467.3 kN.mm respectively, and also by comparing the results of plates 8, 10, and 12 where the energy absorptions were 602.9, 709.4 and 947.9 kN.mm respectively. Moreover, for plates in series designation G plates 13, 14, and 15, energy absorptions were 225.2, 311.5, and 449.6 kN.mm respectively. It is interesting to note that plate 6 in series D exercises high ductility and energy absorption properties, which are very useful in dynamic applications.

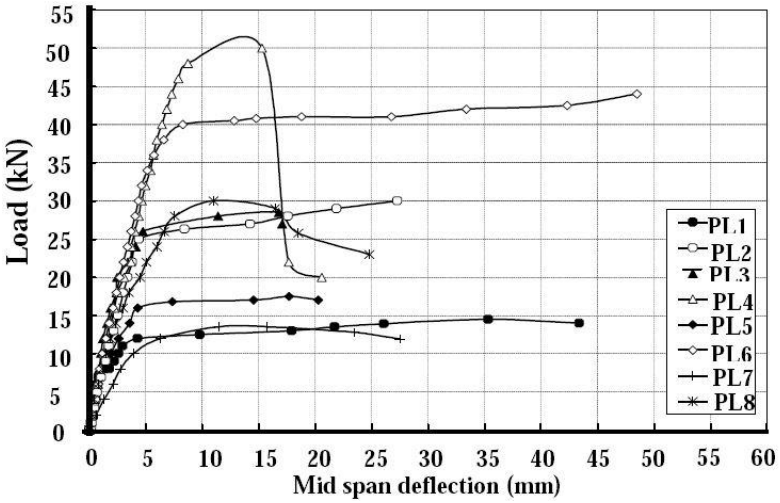

(a) Plates 1 - 8

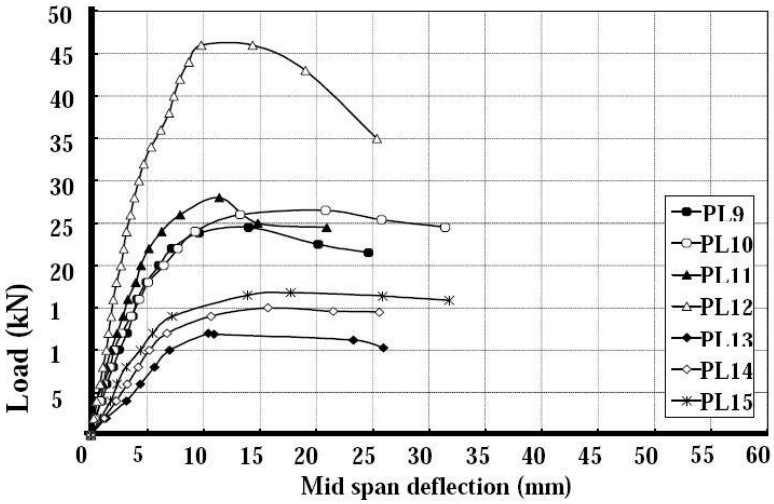

(b) Plates 9 - 15

Fig. 10 Load-deflection curves at mid-span of all test plates

4.1.3 Load- compressive mortar strains curves

The load versus compressive mortar strains are plotted in Fig. 11 for all plates in the seven series, Plates 1 to 15 respectively. The curves display similar characteristics as all the previously examined deformations. The most important observation from load - compressive strain curves is that near failure the maximum compressive strain varies from 0.0286 to 0.00768 strains for plates 1 and 2 reinforced with mild steel bars, series A. In addition, the maximum compressive strain varies from 0.00968 to 0.014 strains for plates reinforced with expanded steel mesh X8 combined with mild steel bars, plates 3 and 4 of series B. Also, one can observed that the maximum compressive strain varies from 0.02658 to 0.0315 strains for plates reinforced with woven steel mesh combined with mild steel bars, plates 5 and 6 of series C, while the maximum compressive strain varies from 0.00696 to 0.01208 strains for plates reinforced with

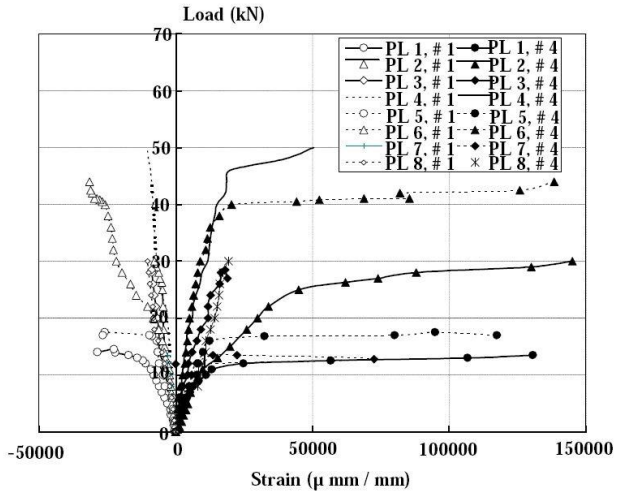

(a) Plates 1 to 8

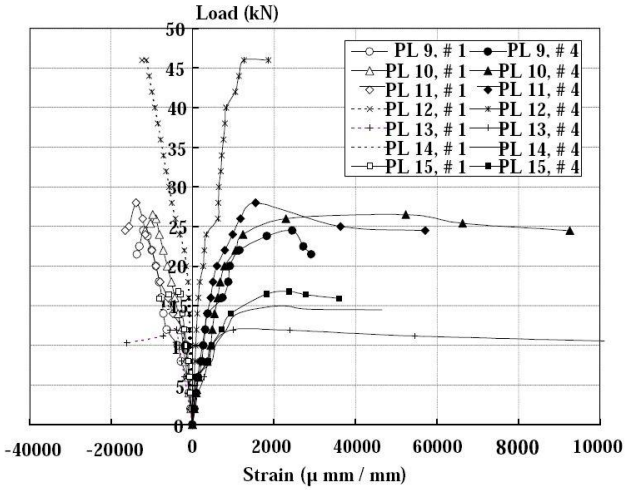

(b) Plates 9 to 15

Fig. 11 Load versus mortar compressive and tensile strains

woven steel mesh and provided with two ribs and core light weight brick, series D, plates 7 and 8. Moreover, the maximum compressive strain varies from 0.0136 to 0.0116 strains for plates reinforced with woven steel mesh and provided with three ribs and core light weight brick, series E, plates 9 and 10, as well as the maximum compressive strain varies from 0.01656 to 0.01328 strains for plates reinforced with woven steel mesh and provided with four ribs and core light weight brick, series F, plates 11 and 12. Finally, the maximum compressive strain were 0.01614, 0.0086, and 0.00764 strains for plates reinforced with woven steel mesh and provided with two, three and four ribs without core material, series G, plates 13, 14, and 15 respectively. As a result, the volume fraction of reinforcement has significant effect on compressive strains. Additionally, the higher volume fraction of the plates exhibits higher strains and this is clearly shown from the load compressive strain curves of the tested plates.

4.1.4 Load- tensile mortar strains curves

The load tensile mortar strains are plotted in Fig. 11 for all plates in the seven series, Plates 1 to 15 respectively. The curves display similar characteristics as all the previously examined deformations. As a result, the most important observation from load - tensile strain curves is that near failure the maximum tensile strain varies from 0.5187 to 0.145 strains for plates reinforced with mild steel bars, series A, plates 1 and 2. In addition, the maximum tensile strain varies from 0.0189 to 0.1272 strains for plates reinforced with expanded steel mesh X8 combined with mild steel bars, series B, plates 3 and 4. Moreover, the maximum tensile strain varies from 0.11744 to 0.1384 strains for plates reinforced with woven steel mesh combined with mild steel bars, series C, plates 5 and 6, while the maximum tensile strain varies from 0.07252 to 0.02592 strains for plates reinforced with woven steel mesh and provided with two ribs and core light weight brick, series D, plates 7 and 8. Also, one can observed that the maximum tensile strain varies from 0.02916 to 0.09256 strains for plates reinforced with woven steel mesh and provided with three ribs and core light weight brick, series E, plates 9 and 10, and also the maximum tensile strain varies from 0.05708 to 0.04244 strains for plates reinforced with woven steel mesh and provided with four ribs and core light weight brick, series F, plates 11 and 12. Finally the maximum tensile strain were 0.1196, 0.04648, and 0.0360 strains for plates reinforced with woven steel mesh and provided with two, three and four ribs without core material, series G, plates 13, 14, and 15 respectively. It can be concluded that the volume fraction of reinforcement gives significant effect on tensile strains. Also, the higher volume fraction of the plates exhibits higher strains. This is clearly shown from the load tensile strain curves of the tested plates. In addition, the measured tensile mortar strains after first crack include crack widths and they can be used for comparison purposes only. Fig. 11 shows load versus mortar compressive and tensile strains for all the tested plates.

4.1.5 Failure modes

For all series designations of all the tested plates flexural failure occurred except plate 8 in series D and plate 12 in series F diagonal cracks occurred. Failure of the test specimens occurred due to reaching the ultimate stress of the reinforcing steel mesh.

However, none of steel mesh was ruptured, which indicates that the strain in the steel mesh did not reach the ultimate strain of the steel mesh. After the end of each test, the specimen was removed from the testing machine and the mortar cover was removed to expose the reinforcing steel mesh. The visual investigation of the steel mesh confirmed that none of the bars were ruptured. For Plate 8, which belong to designation D, consists of two ribs and reinforced with steel mesh at both top and bottom. Additionally, for plate 12, which belong to designation F, composed of four ribs and reinforced with steel mesh at the top and steel mesh at the bottom. Diagonal tension crack developed in each of the two plates 8 and 12 and failure occurred due to reaching the shear strength of the two specimens. Cracks differed in width, number, and propagation directions according to the physical properties of each designation. In the next section the crack patterns and distributions are discussed for each designation separately.

4.1.6 Cracking patterns

Fig. 12 shows side views of crack patterns of all the tested plates. For designation (A), flexural cracks developed near the mid-span of the specimens of this designation at a load of approximately 8 kN, for plate 1 and 15 kN for plate 2. With the increase of the load, the cracks propagated vertically and new flexural cracks were developed rapidly. As the specimens approached their

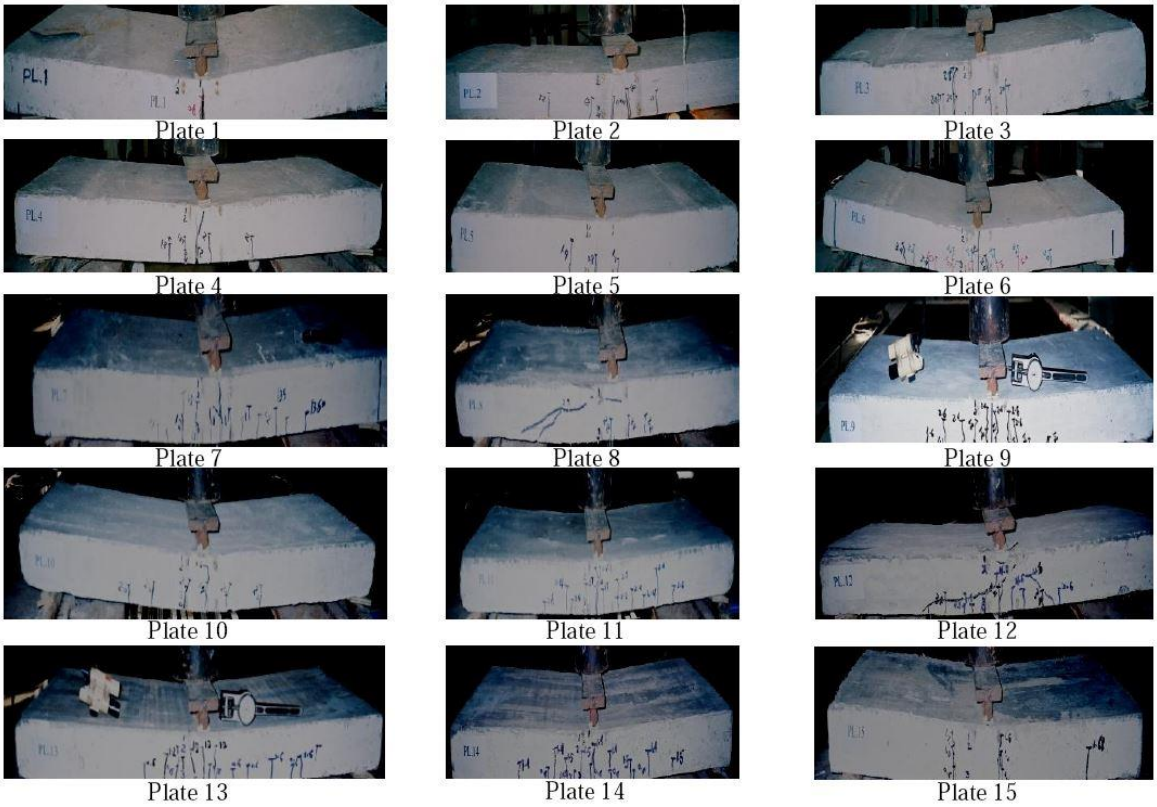

Fig. 12 Side cracking patterns of all the tested plates

failure load, the cracks started to propagate wider.

The crack width was measured for all tested plates. It was observed that the cracks were very wide as result of employing steel bars. For designation (B) plate 3 and 4, it is interesting to note that vertical flexural cracks started to develop close to the center of the span. As the load increased, more cracks started to develop and the crack at mid-span started to propagate vertically towards the top surface of the specimen, while most of the developed cracks did not continue propagating.

The crack widths were much less than those of designation (A). This could be attributed to the effect of steel mesh in controlling the crack width. For series designation C, plates 5 and 6, plate 5, which was reinforced with one layer of woven steel mesh combined with skeletal steel bars, the flexural cracks were less than series A. At failure of Plate 6, which was reinforced with two woven steel layers and combined with steel bars, very narrow cracks were observed. For series designation D, plates 7 and 8, it is interesting to note that very fine vertical cracks were developed than the previous designations and the cracks were uniformly distributed along the middle 2/3 of the span. The observed crack widths were much less than those of designations A and B. This could be attributed to the effect of the steel mesh in controlling the crack width. For plate 8, the flexural cracks started to turn diagonally as the load approached the failure load and one diagonal crack developed near the end. For series designation E, plates 9 and 10, at failure, very narrow flexural cracks were developed compared with the plates in the previous series. For series designation F, plates 11 and 12, the number of developed cracks was more than the previous

Table 3 Comparison of load values between the experimental and FE simulation results

Designation	Plate No.	1st crack load (kN)		Serviseability load (kN)		Ultimate load (kN)	
		Exp.*	FE	Exp.	FE	Exp.	FE
A	PL1	0.80	0.73	0.77	0.70	1.45	1.45
	PL2	1.54	1.95	1.73	1.61	3.00	3.00
B	PL3	2.00	1.85	1.64	1.47	2.85	2.85
	PL4	2.00	3.26	4.28	2.82	5.00	5.02
C	PL5	0.80	0.92	0.95	0.97	1.75	2.05
	PL6	2.00	1.07	2.61	3.00	4.40	5.31
D	PL7	1.20	0.95	0.77	0.65	1.35	1.40
	PL8	2.40	2.06	1.78	1.58	3.00	3.02
E	PL9	1.40	1.64	1.44	1.22	2.45	2.45
	PL10	1.60	1.51	1.56	1.65	2.65	3.14
F	PL11	1.40	1.82	1.66	1.44	2.80	2.80
	PL12	3.40	3.43	2.77	2.84	4.60	5.05
G	PL13	0.60	0.56	0.65	0.50	1.12	1.25
	PL14	0.80	0.75	0.88	0.72	1.46	1.66
	PL15	0.80	0.91	0.97	0.94	1.68	2.02

***** Experimental

designations and the cracks were uniformly distributed along the middle 2/3 of the span.

The observed crack widths were much less than those of the previous series. Flexural cracks occurred for plate 11 while failure of plate 12 occurred due to reaching the shear strength of the specimens. The reinforcing steel meshes did not rupture for this designation and superior crack pattern was obtained at failure with very fine crack widths. This could be attributed to increasing the number of ribs from three to four, which resulted a very stiff plates compared with the other series. For series designation G comprise plates 13, 14, and 15 manufactured without light bricks, the reinforcement in the webs provided resistance to the shear stress and consequently prevented the development of the diagonal cracks. In the mean time, this U-shape reinforcement controlled the vertical propagation of the cracks.

4.2 Comparison between experimental and FE simulation results

The comparison between experimental and FE simulation results; 1st crack load, serviceability load, ultimate load, 1st crack deflection, deflection at serviceability load, mid span deflection at the ultimate load and ductility ratio are illustrated in Tables 3 and 4. Figs. 13 to 22 present the applied load-mid span deflection, and the applied load-strain curves; respectively as obtained from the experimental and theoretical results for the all test ferrocement plates. The first crack load was determined as the first deviation from linearity of load deflection curve. The comparison between the experimental and theoretical cracking patterns for all tested specimens is presented in Fig. 23. It can be clearly seen that the observed cracking patterns for all the tested specimens are flexural cracks and they started in appearing at the plate mid-span. Then they developed rapidly from the tension side towards the compression side and propagated along the plate span with increasing the

Table 4 Comparison of deflection values between the experimental and FE simulation results

Designation	Plate No.	1st crack deflection (mm)		Deflection at Serviseability load (mm)		Maximum deflection (mm)		Ductility ratio	
		Exp.*	FE	Exp.	FE	Exp.	FE	Exp.	FE
A	PL1	1.80	1.37	1.30	1.09	35.4	38.52	19.9	28.12
	PL2	2.60	2.30	2.90	1.51	27.3	24.87	10.6	10.81
B	PL3	2.50	3.30	2.00	1.74	16.8	16.71	6.80	5.06
	PL4	3.10	3.41	4.70	2.42	15.3	15.68	4.90	4.59
C	PL5	1.40	1.73	1.80	2.35	17.7	17.1	12.6	9.77
	PL6	2.70	1.37	3.70	16.2	48.5	38.5	17.8	28.1
D	PL7	6.30	4.61	2.70	1.70	15.7	15.1	2.50	3.28
	PL8	6.00	2.70	3.50	1.25	11.0	11.91	1.80	4.40
E	PL9	3.70	3.78	3.80	1.80	14.0	14.63	3.80	3.87
	PL10	4.30	3.44	4.20	4.84	20.9	19.56	4.80	5.69
F	PL11	2.90	2.81	3.50	1.70	11.4	11.41	4.00	4.06
	PL12	5.30	3.98	3.80	2.35	14.4	14.82	2.70	3.70
G	PL13	4.00	3.90	4.40	3.10	23.3	22.32	5.80	5.72
	PL14	4.20	1.90	4.60	1.70	15.7	16.25	3.70	8.55
	PL15	4.40	2.51	4.30	2.95	17.7	16.10	4.00	5.46

* Experimental

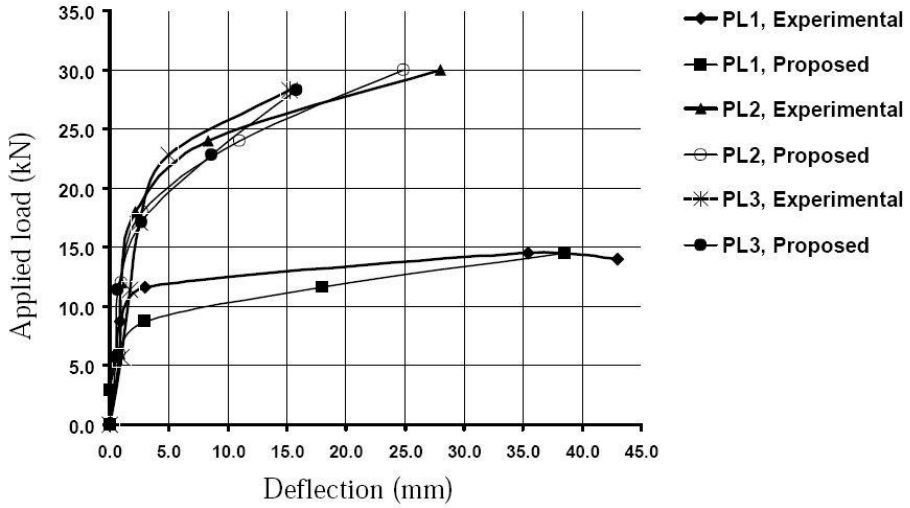

Fig. 13 Curve applied load in function of deflection of experimental and proposed models PL1, PL2, and PL3

applied load. Allover, it can be observed that in the two control plates (PL1 and PL2), shear cracks are generated near the failure load. Also, this figure showed that few flexural cracks developed in other specimens and their widths at the failure load are seemed to be large than the cracks width in the control plates. Additionally, the crack widths are increased with increasing the number of layers of refinement as indicated in the Fig. 23.

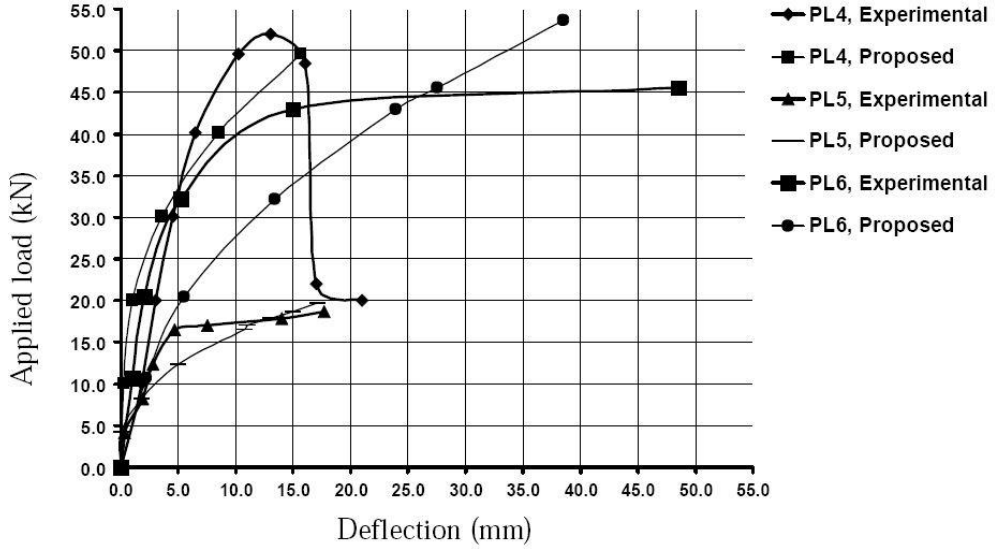

Fig. 14 Curve applied load in function of deflection of experimental and proposed models PL4, PL5, and PL6

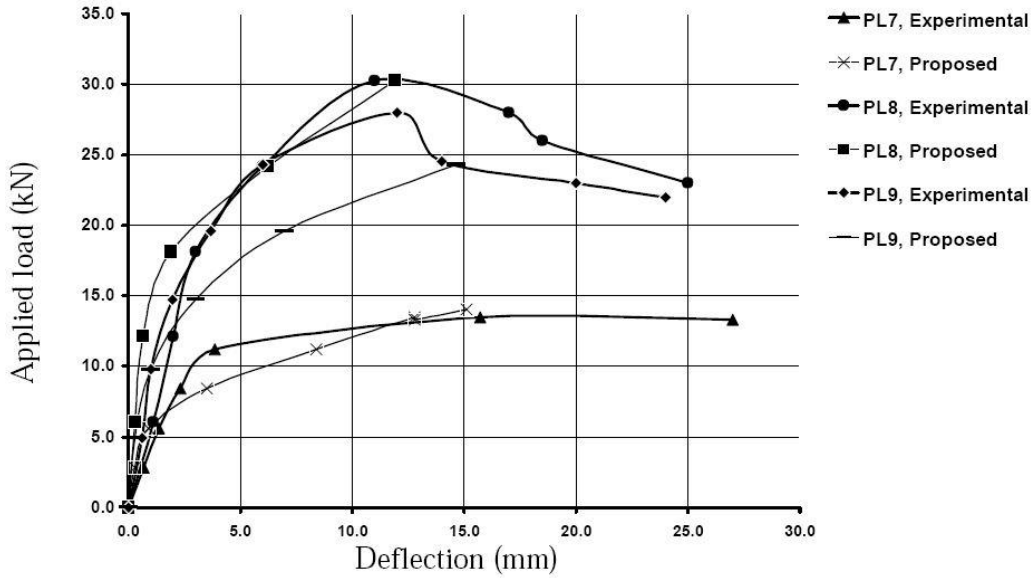

Fig. 15 Curve applied load in function of deflection of experimental and proposed models PL7, PL8, and PL9

From these comparisons, it can be concluded that the FE simulations give accurate results in comparing with the experimental results. In addition, these comparisons indicate a good agreement in slope of curves in the linear stage. For nonlinear stage, and due to the possibility of the inaccuracy in modeling the post yield behavior of steel rebar material, there is somewhat none agreement between the finite element results and those of experimental results.

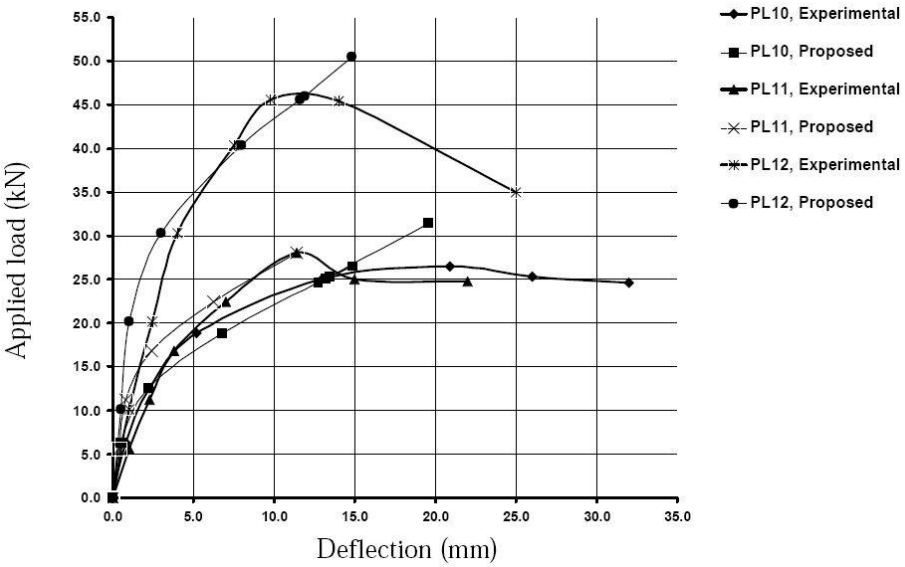

Fig. 16 Curve applied load in function of deflection of experimental and proposed models PL10, PL11, and PL12

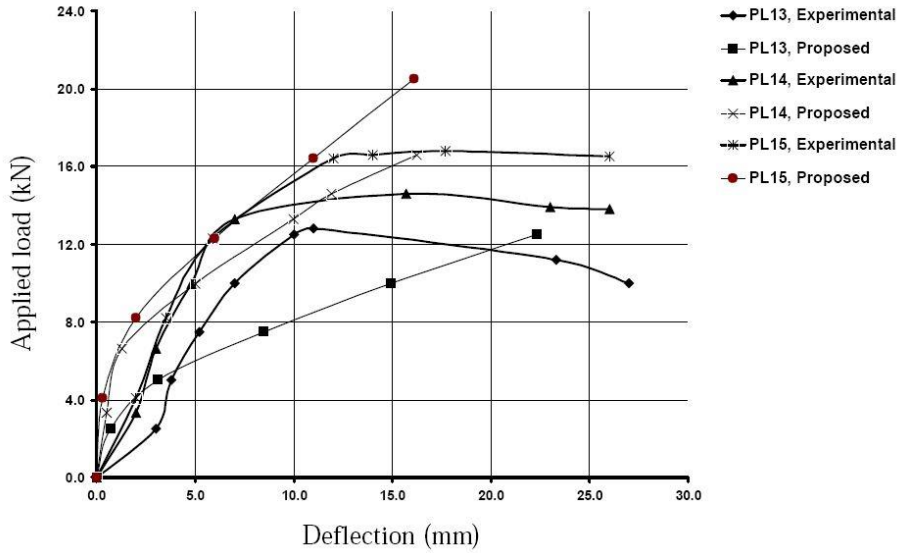

Fig. 17 Curve applied load in function of deflection of experimental and proposed models PL13, PL14, and PL15

5. Parametric studies

To further improve the understanding of the flexural behavior of Ribbed Plates reinforced with composite material, parametric studies were performed to investigate the impact of the increase of the tested plate dimensions, upon the strength capacity of the models having ferrocement

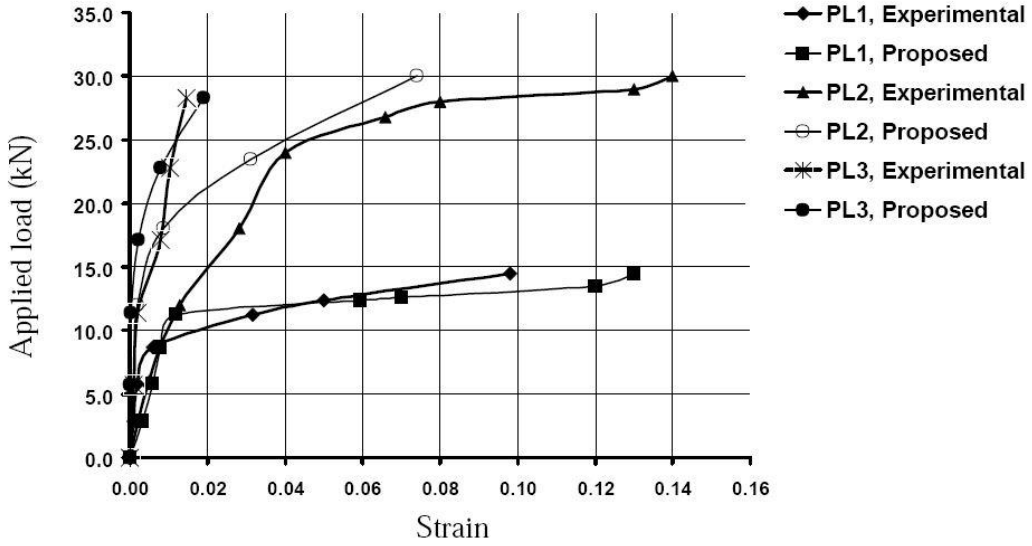

Fig. 18 Curve applied load in function of strain of experimental and proposed models PL1, PL2, and PL3

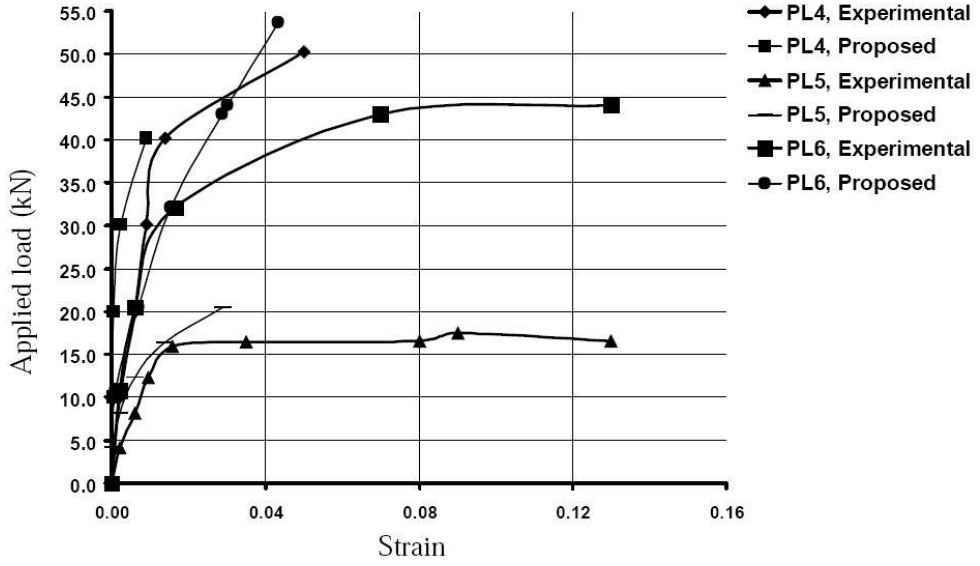

Fig. 19 Curve applied load in function of strain of experimental and proposed models PL4, PL5, and PL6

reinforcement. The study was conducted on four proposed models of lengths 1600 mm, 2000 mm and 2400 mm respectively.

Figs. 24 and 25 compare the results obtained for the ultimate load and the maximum deflection values respectively. It has to be noted that in case of an increase of the length by an amount of

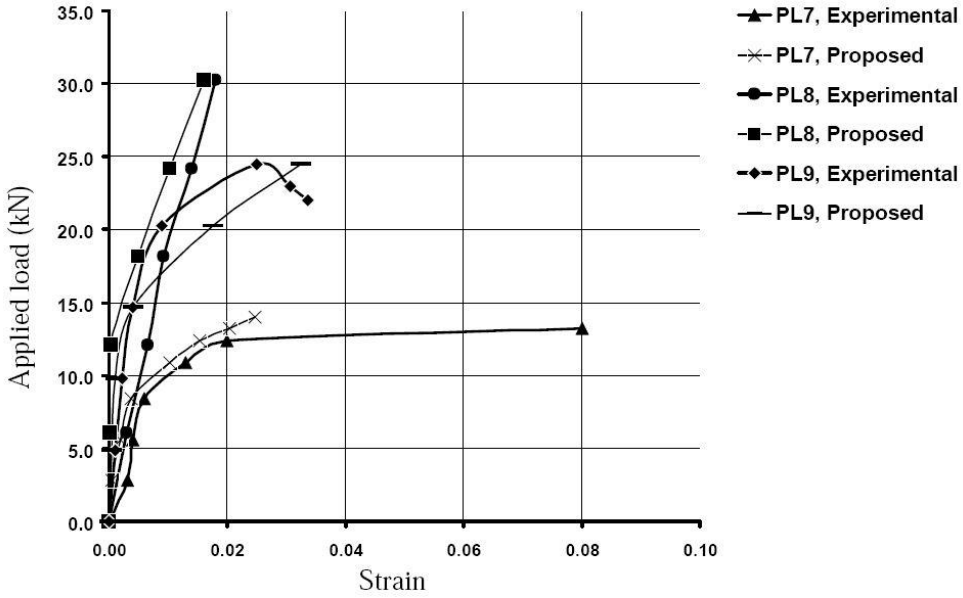

Fig. 20 Curve applied load in function of strain of experimental and proposed models PL7, PL8, and PL9

25 %, the FE ultimate load decrease by an amount of (11-18) % according to the type of plate, and also the FE maximum deflection increase by an amount of (40-200) %.

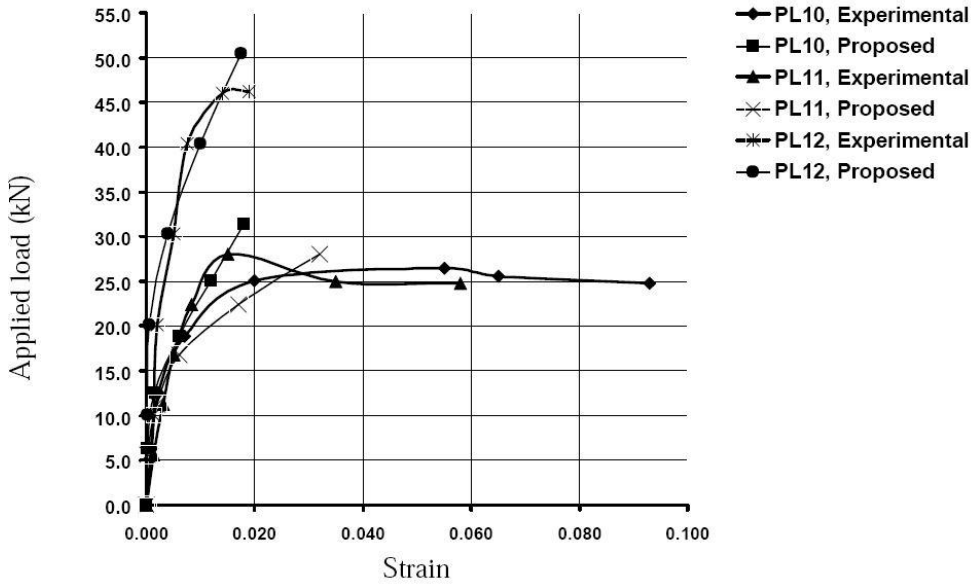

Fig. 21 Curve applied load in function of strain of experimental and proposed models PL10, PL11, and PL12

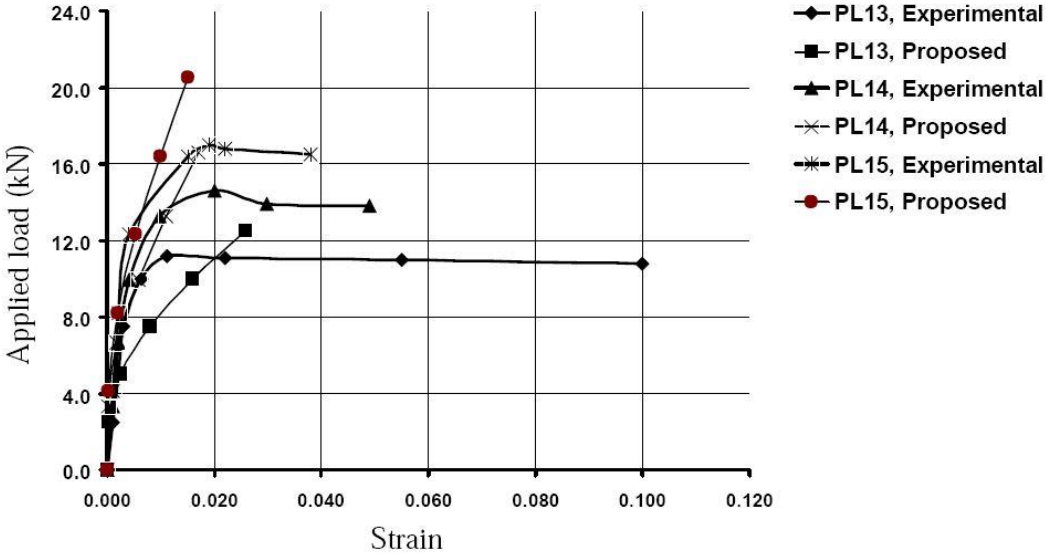

Fig. 22 Curve applied load in function of strain of experimental and proposed models PL13, PL14, and PL15

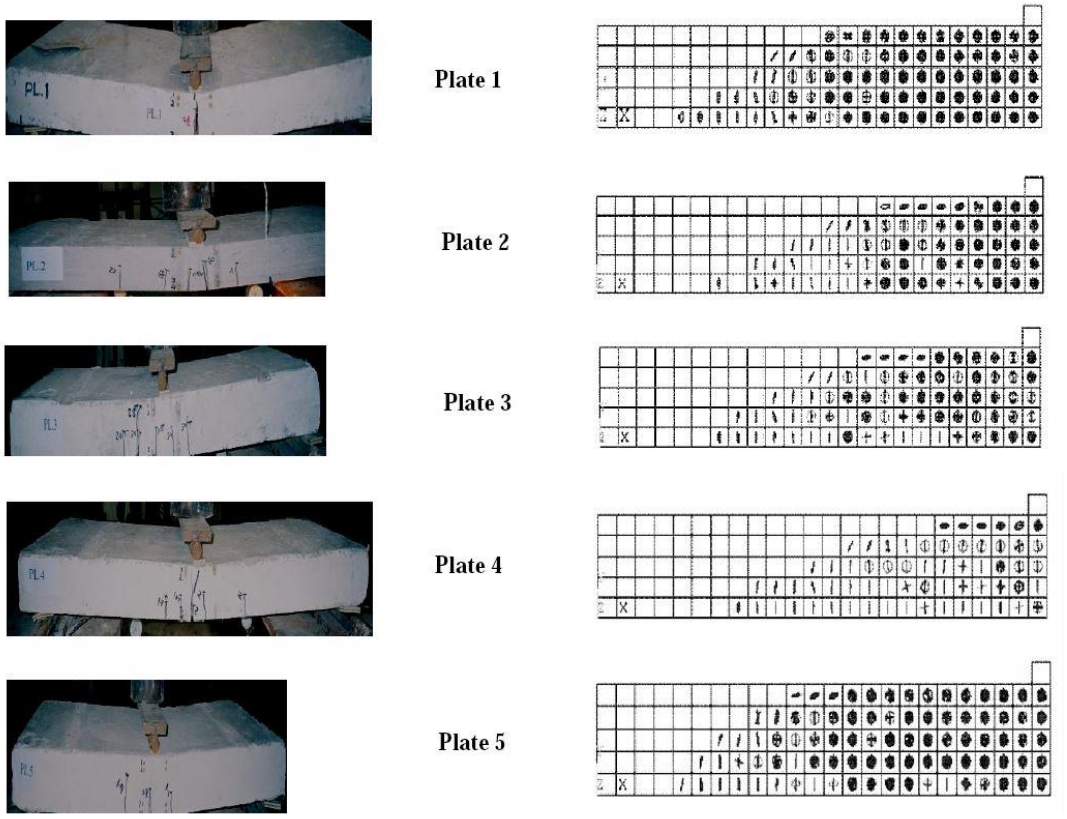

Fig. 23 Experimental and FE side cracking patterns of all the tested Plates

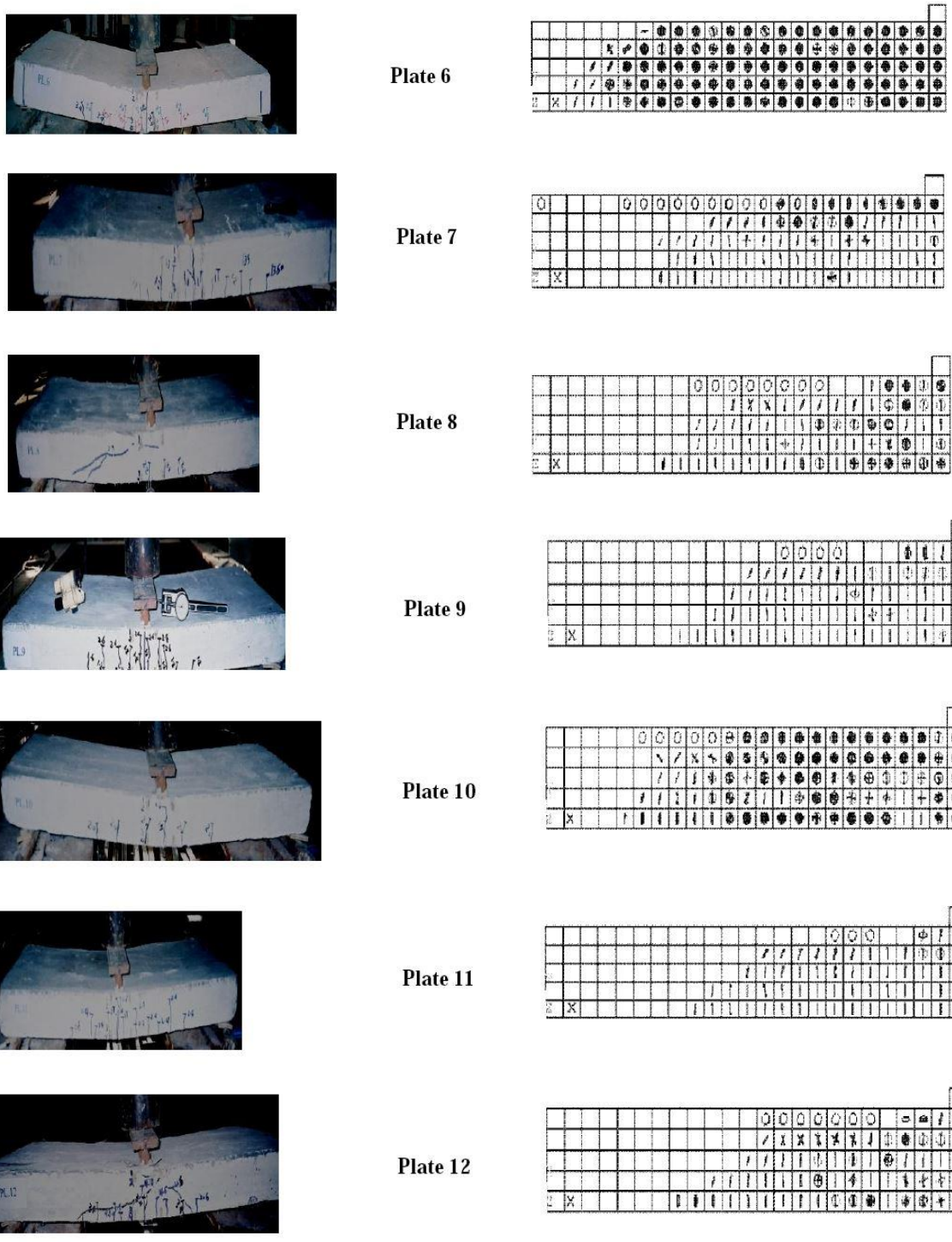

Fig. 23 Continued

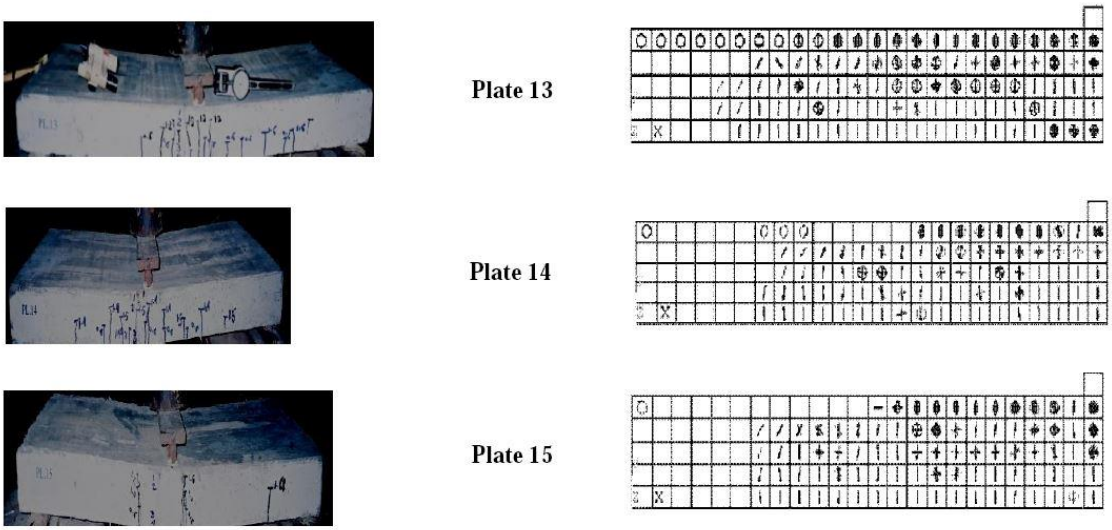

Fig. 23 Continued

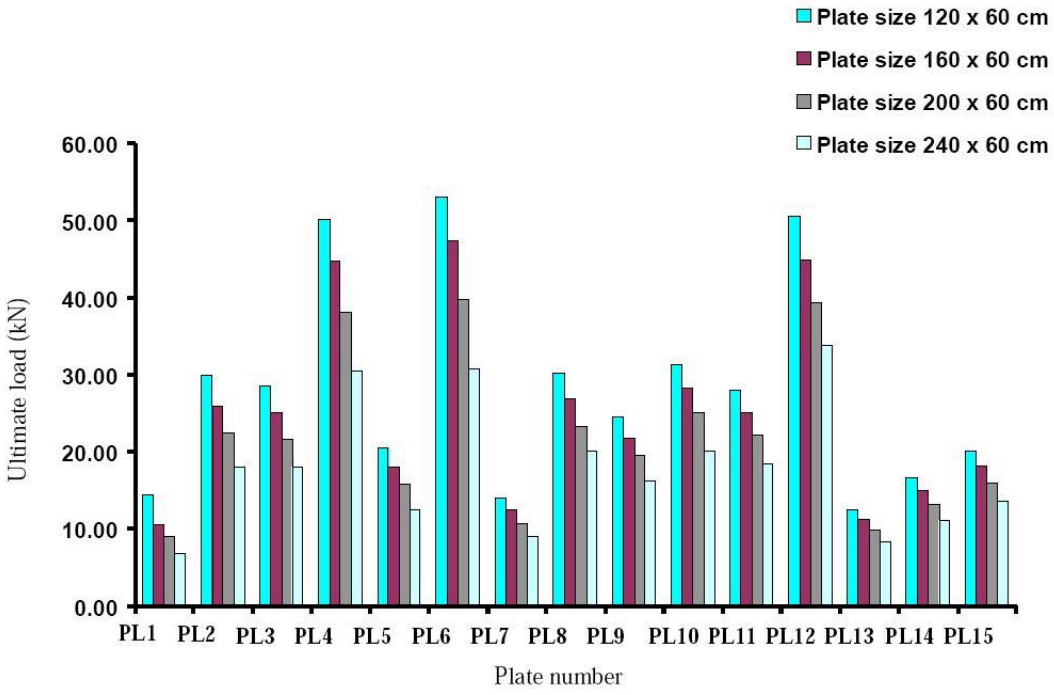

Fig. 24 Ultimate load of selected models with varying plate dimensions

6. Conclusions

The observations during the experimental and FE model delivered valuable information concerning the flexural behavior of ferrocement Ribbed Plates reinforced with composite material.

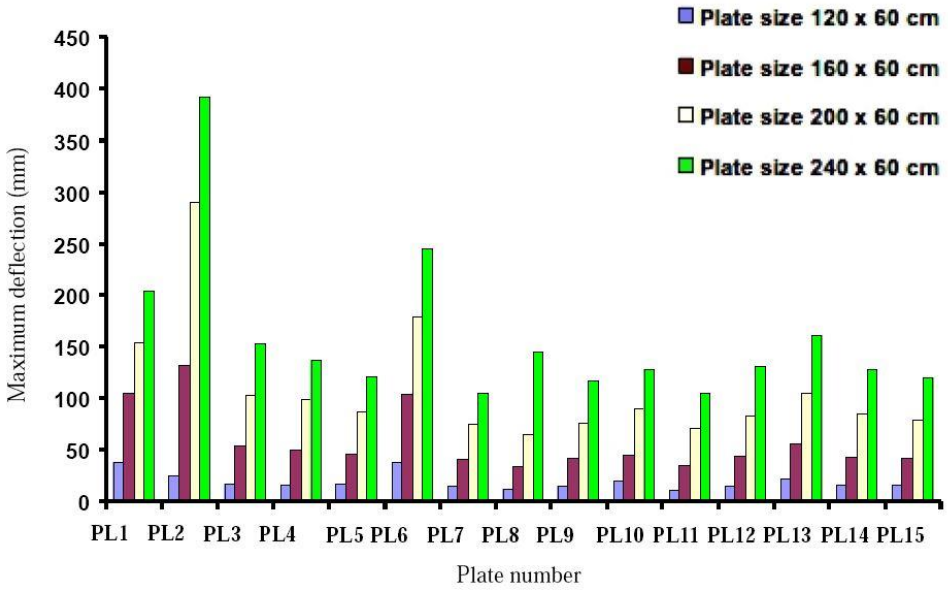

Fig. 25 Maximum deflection of selected models with varying plate dimensions

Based on the experimentally available results and the FE numerical study, the following conclusions can be drawn as follows:

1. The developed ribbed ferrocement plates emphasized better deformation characteristics and high serviceability loads, crack resistance and energy absorption, but it leads to decrease the ductility.
2. Using two layers of expanded metal mesh in reinforcing ferrocement plates, clearly increase the ultimate moment and improve the energy absorption than obtained when using skeletal steel bars.
3. Irrespective of the type of expanded metal mesh, woven steel mesh using two mild steel bars with one layer expanded metal mesh leads to improve ductility ratio and energy absorption and consequently increase ultimate moment than that obtained when using two-layers expanded metal mesh.
4. There is a great saving of weight by employing light weight brick leading to easy construction especially for weak soil foundations.
5. A numerical FE model based on the finite element theory can be used to investigate the flexural behavior of ferrocement Ribbed Plates reinforced with composite material, leading to a good agreement when comparing to available full-scale test data.
6. The comparison of the crack patterns obtained by the FE and experimental models leads to an identical crack propagation for the two approaches up to failure. The inclination of the failure surfaces and the concentration of cracks of all plates were the same in both patterns.
7. An increase in the FE strength capacity values of 15% compared to the experimentally available data was concluded, leading to a good agreement between them.
8. Parametric study was performed in order to look at the effect of changing the plate length on the strength capacity of the ferrocement plate. It can be noted that the increase of the length of the plate model lead to a decrease of the strength capacity, and an increase of the maximum

deflection.

References

Abdul-Fataha, S. (2014), "Structural behavior of concrete beams reinforced with innovative materials", M. Sc. Thesis, Minufiya University, Shebin El-Kom, Egypt.

Aboul-Anen, B., El-Shafey, A. and El-Shami, M. (2009), "Experimental and analytical model of ferrocement slabs", *Int. J. Recent Trend. Eng.*, **1**(6), 25-29.

ACI 549R-97 (1993), State-of-the-Art Report on Ferrocement, American Concrete Institute, Detroit, MI 48219, USA.

Acma, L., Dumpasan, G., Salva, M., Mansaguiton, M., Supremo, R. and Daquiado, N. (2015), "Flexural strength and ductility behavior of ferrocement I-beam", *Mindanao J. Sci. Tech.*, **13**, 99-108.

Al-Kubaisy, M.A. and Jumaat, M.Z. (2000), "Flexural behavior of reinforced concrete slabs with ferrocement tension zone cover", *J. Constr. Build. Mater.*, **14**, 245-252.

Al-Rifaei, W.N. and Hassan, A.H. (1994), "Structural behavior of thin ferrocement one-way bending elements", *J. Ferroc.*, **24**(2), 115-126.

Ali, A. (1995), "Applications of ferrocement as a low cost construction material in Malaysia", *J. Ferroc.*, **25**(2), 123-128.

ANSYS "Help and manual" (2006), 12th Editor, ANSYS Inc, PA, USA.

E.C.P. (2007), Egyptian code of practice: design and construction for reinforced concrete structures, research Centre for Houses Building and Physical Planning, Cairo, Egypt, No. 203.

El-Halfawy, E. (2003), "Flexural behavior of ferrocement deck bridges", M.Sc. Thesis, Minufiya University, Shebin El-Kom, Egypt.

El-Sakhawy, Y. (2000), "Structural behavior of ferrocement roof elements", B.Sc. Thesis, Minufiya University, Shebin El-Kom, Egypt.

Elavenil, S. and Chandrasekar, V. (2007), "Analysis of reinforced concrete beams strengthened with ferrocement", *Int. J. Appl. Eng. Res.*, **2**(3), 431-440.

Eskandari, H. and Madadi, A. (2015), "Investigation of ferrocement channels using experimental and finite element analysis", *Int. J. Eng. Sci. Tech.*, **18**(4), 769-775.

Fahmy, E.H. and Shaheen, Y.B. (1994), "Laminated ferrocement for strengthening and repairing of reinforced concrete beams", *Proceeding of Annual Conference of CSCE*, 475-483.

Fahmy, E.H., Ezzat, H., Shaheen, Y.B. and Abou Zeid, M.N. (2004), "Development of ferrocement panels for floor and wall construction", *Proceedings of the 5th Structural Specialty Conference of the Canadian Society for Civil Engineering*, Saskatoon, Saskatchewan, Canada.

Fahmy, E.H., Ezzat, H., Shaheen, Y.B., Abou Zeid, M.N. and Abdel Naby, A.M. (2005), "Permanent ferrocement forms: a viable alternative for construction of concrete bBeams", *Proceedings of the 30th Conference on Our World in Concrete and Structures*, Singapore, 249-256.

Fahmy, E.H., Shaheen, Y.B. and Korany, Y.S. (1997), "Use of ferrocement laminates for repairing reinforced concrete slabs", *J. Ferroc.*, **27**(3), 219-232.

Fahmy, E.H., Shaheen, Y.B. and Korany, Y.S. (1999), "Repairing reinforced concrete columns using feroocement laminates", *J. Ferroc.*, **29**(2), 115-124.

Fahmy, E.H., Shaheen, Y.B., Abou-Zeid, M.N. and Abdel-Naby, A.M. (2005), "Permanent ferrocement forms: a viable alternative for construction of concrete beams", *Proceedings of the 30th Conference on Our World in Concrete and Structures*, Singapore, 249-256.

Fahmy, E.H., Shaheen, Y.B.I. and Abou-Zeid, M.N. (2004), "Development of ferrocement panels for floor and wall construction", *Proceedings of the 5th Structural Specialty Conference of the Canadian Society for Civil Engineering*, Saskatoon, Saskatchewan, Canada.

Fahmy, E.H., Shaheen, Y.B.I. and Korany, Y.S. (1999), "Repairing reinforced concrete columns using ferrocement laminates", *J. Ferroc.*, **29**(2), 115-124.

Hafiz, A. (2012), "Structural behaviour of ferrocement channels beams", M. Sc. Thesis, Minufiya University, Shebin El-Kom, Egypt.
Hoque, M. (2006), "3D nonlinear mixed finite-element analysis of RC beams and plates with and without FRP reinforcement", M.Sc. Thesis, University of Manitoba, Winnipeg, Manitoba, Canada.
Jumaat, M. and Alam, A. (2006), "Flexural strengthening of reinforced concrete beams using ferrocement laminate with skeletal bars", *J. Appl. Sci. Res.*, **2**(9), 559-566.
Kaish, M.A., Alam, A.B., Jamil, M.R., Zain, M.F. and Wahed, M.A. (2012), "Improved ferrocement jacketing for restrengthening of square RC short column", *J. Constr. Build. Mater.*, **36**, 228-237.
Mays, G.C. and Barnes, R.A. (1995), "Ferrocement permanent formwork as protection to reinforced steel mesh concrete", *J. Ferroc.*, **25**(4), 331-345.
Mourad, S.M. and Shannag, M.J. (2012), "Repair and strengthening of reinforced concrete square columns using ferrocement jackets", *Cement Concrete Compos.*, **34**, 288-294.
Robles-Austriaco, L., Pama, R.P. and Valls, J. (1981), "Ferrocement an innovative technology for housing", *J. Ferroc.*, **11**(1), 23-47.
Sakthivel, P. and Jagannathan, A. (2012), "Fibrous ferrocement composite with PVC-coated weld mesh and bar-chip polyolefin fibers", *Int. J. Geom.*, **3**(2), 381-388.
Sakthivel, P. and Jagannathan, A. (2012), "Study of flexural ferrocement and thin reinforced cement behavior of ferrocement slabs reinforced with PVC-coated weld mesh", *Int. J. Eng. Res. Develop.*, **1**(12), 50-57.
Shaheen, Y., Eltaly, B. and Abdul-Fataha, S. (2014), "Structural performance of ferrocement beams reinforced with composite materials", *Struct. Eng. Mech.*, **50**(6), 817-834.
Shaheen, Y., Safan, M. and Abdalla, M. (2013), "Structural behavior of composite reinforced ferrocement plates", *J. Concrete Res. Lett.*, **4**(3), 621-638.
Shaheen, Y., Soliman, N. and Hafiz, A. (2013), "Structural behavior of ferrocement channels beams", *J. Concrete Res. Lett.*, **4**(3), 621-638.
Shaheen, Y.B.I., Eltaly, B. and Kameel, M. (2013), "Experimental and analytical investigation of ferrocement water pipe", *J. Civil Eng. Constr. Tech.*, **4**(4), 157-167.
Shannag, M.J. and Mourad, S.M. (2012), "Flowable high strength cementitious matrices for ferrocement applications", *Constr. Build. Mater.*, **36**, 933-939.
Singh, G. (2006), "Finite element analysis of reinforced concrete shear walls", M.Sc. Thesis, Deemed University, India.
Singh, V., Bansal, P. and Kumar, M. (2015), "Experimental studies on strength and ductility of ferrocement jacketed RC beam-column joints", *Int. J. Civil Struct. Eng.*, **5**(3), 199-205.
Xiong, G.J., Wu, X.Y., Li, F.F. and Yan, Z. (2011), "Load carrying capacity and ductility of circular concrete columns confined by ferrocement including steel bars", *J. Constr. Build. Mater.*, **25**, 2263-2268.

CC

Nomenclature

V_{rL}	=	volume fraction in ferrocement element
E_c	=	modulus of elasticity of concrete
F_{cu}	=	cube characteristic compressive strength of concrete
ε	=	concrete strain
ε_o	=	corresponding concrete strain at maximum stress
$P_{service}$	=	serviceability load
P_{ult}	=	ultimate load